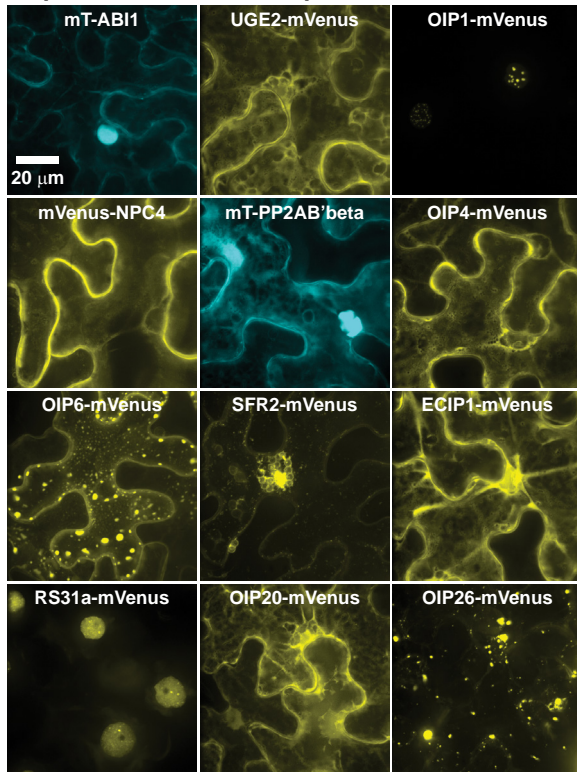
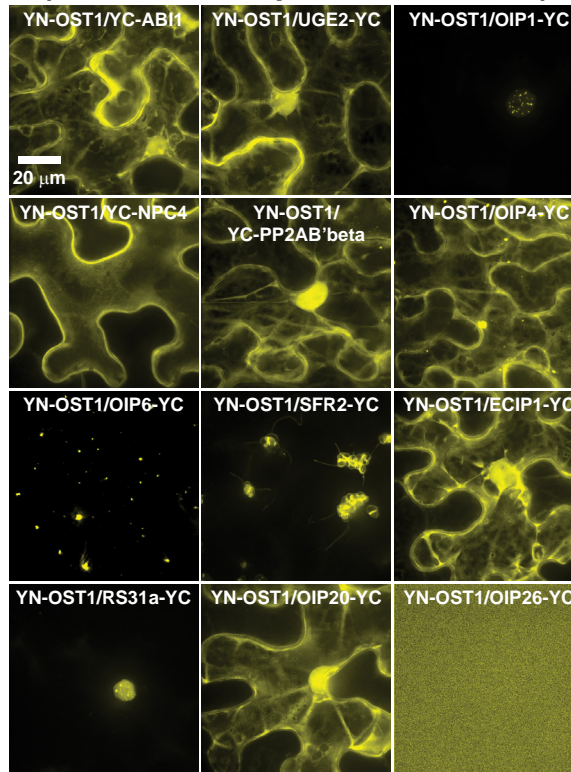


Supplemental Figure S1. Western blot of HF-lines and control co-IP experiments. A, Anti-FLAG western blot confirms expression of indicated constructs (top panel) and PageBlue loading control (bottom panel). B, Western blots of HF-tagged proteins (anti-FLAG, top panel) and mVenus-tagged proteins (anti-GFP, bottom panel) after co-expression in *N. benthamiana* (Input) and anti-FLAG immunoprecipitation (IP) of HF-tagged proteins. Note that OST1-HF cannot efficiently co-purify mVenus-ABI1. However, HF-ABI1 can efficiently co-purify mVenus-OST1.

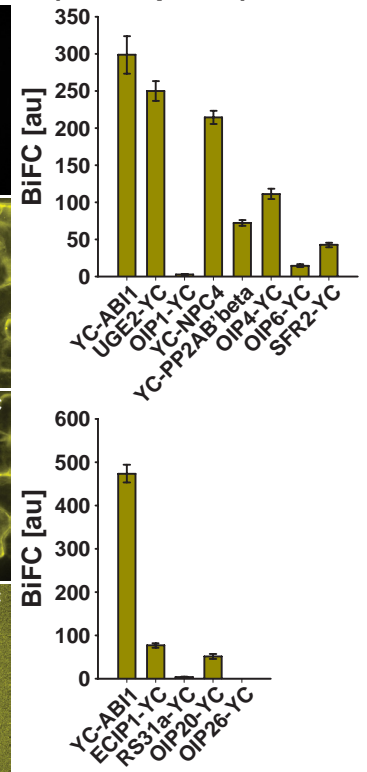
A (OIP localizations)



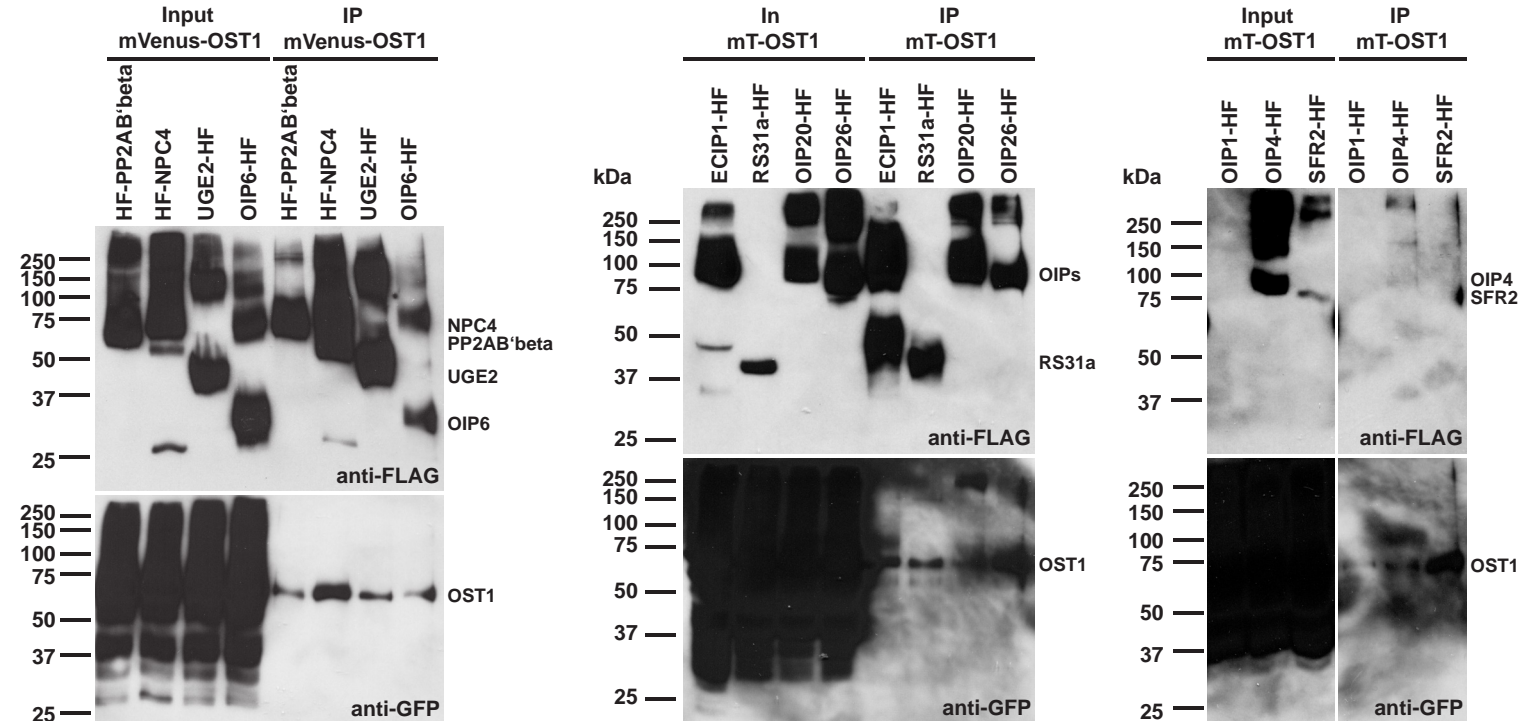
B (OST1-OIP complex localizations)



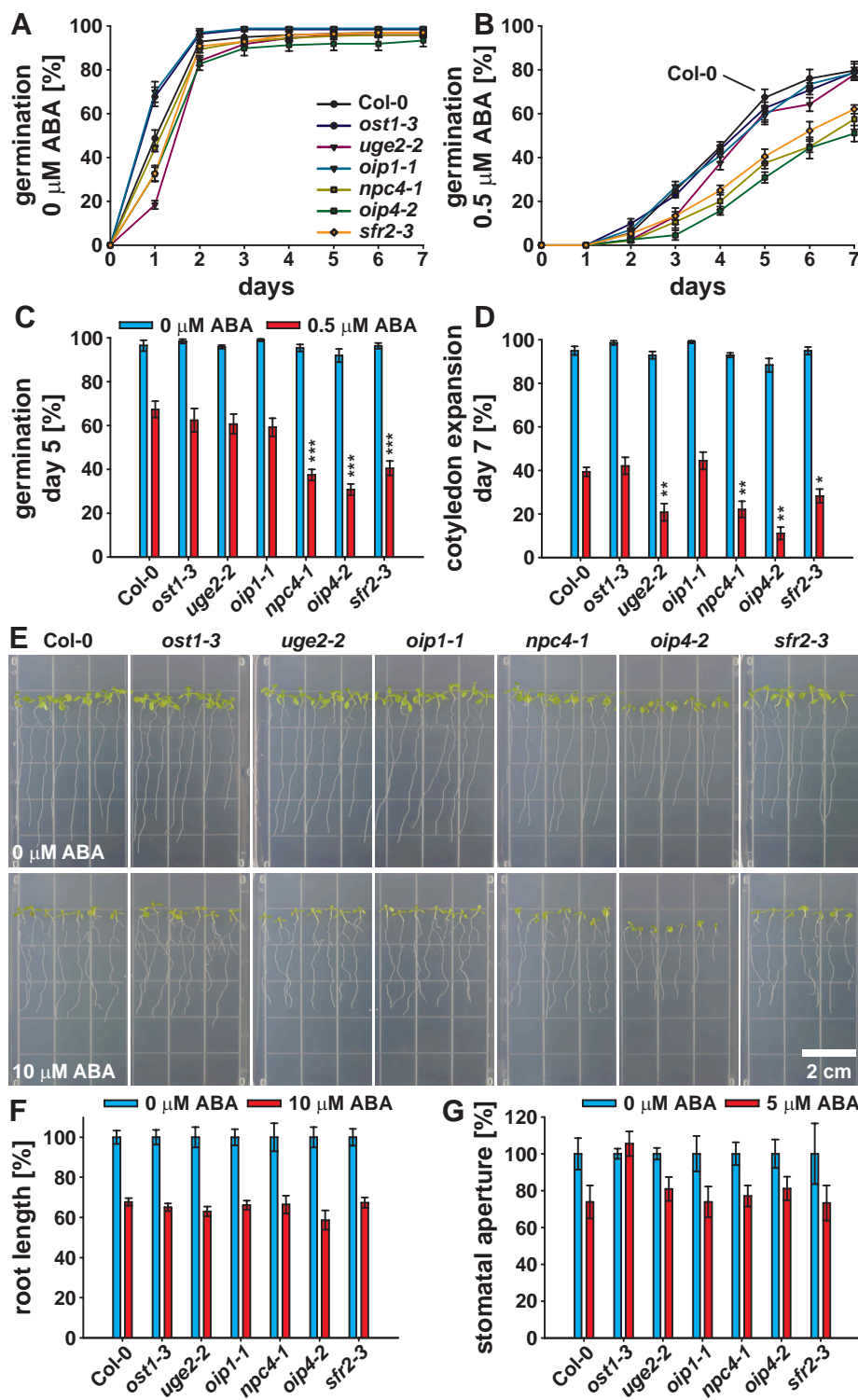
C (BiFC quant.)



D (OST1-OIP co-IPs)

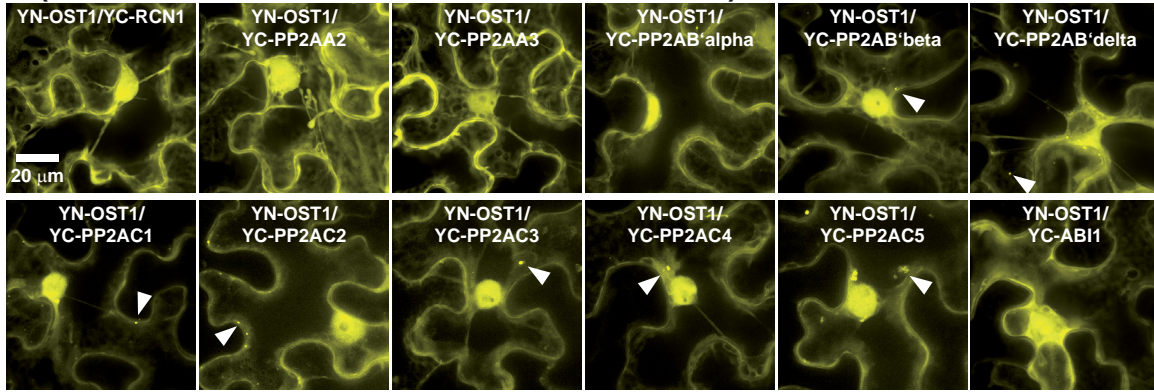


Supplemental Figure S2. Subcellular localizations and interaction analyses of OST1 with OST1-interacting proteins. A, Subcellular localizations of indicated (mT)urquoise- or mVenus-tagged OST1-interacting proteins (OIPs) after transient expression in *N. benthamiana*. B, Subcellular localizations of BiFC complexes of YN-OST1 with YC-tagged OIPs. A and B, Maximum projections of 32-plane z-stacks. C, BiFC quantifications (means \pm SEM, $n = 10$ images). Note that BiFC data are derived from two separate experiments. BiFC emissions of OIP1, OIP6, SFR2 and RS31a appear weak in the quantifications due to their restricted localization pattern and due to acquisition and quantification of entire low magnification images under identical conditions for the indicated construct combinations (see main text and Materials and Methods). D, Western blots of HF-tagged OIPs (anti-FLAG, top panel) and mVenus- or mT-OST1 (anti-GFP, bottom panel) after co-expression in *N. benthamiana* (Input) and anti-FLAG immunoprecipitation (IP) of HF-tagged OIPs.



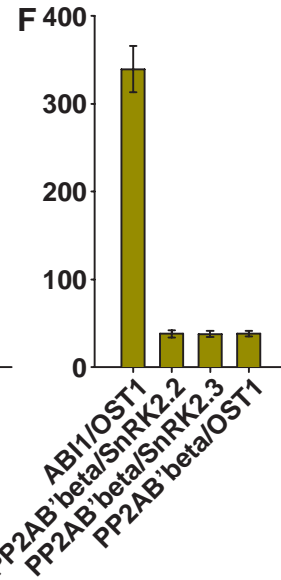
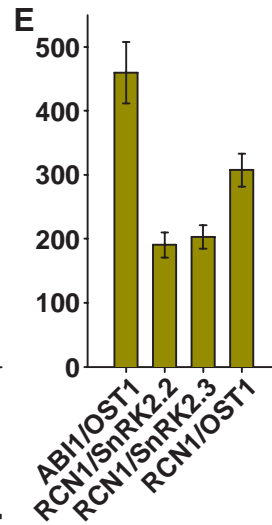
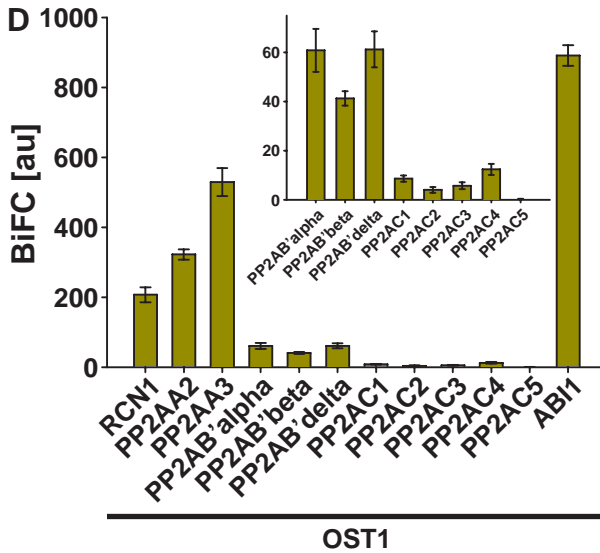
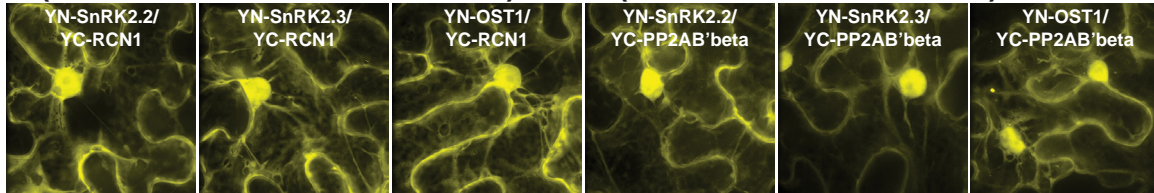
Supplemental Figure S3. OST1-interacting protein mutants exhibit a reduced ABA sensitivity during seed germination. A and B, Time-dependent seed germination of Col-0 and indicated *oip* mutants in presence of (A) 0 μM ABA and (B) 0.5 μM ABA. C and D, Seed germination on (C) day 5 after stratification and (D) cotyledon expansion on day 7 after stratification in the presence of 0 μM ABA (blue bars) and 0.5 μM ABA (red bars). A to D, Means \pm SEM, $n = 4$ with 49 seeds/ n and normalized to the seed count. E, 4-day-old seedlings were transferred to 0.5 MS agar plates supplemented with 0 μM ABA (top row) or 10 μM ABA (bottom row) and grown for additional 5 days. F, Root growth of seedlings shown in (E) in the presence of 0 μM ABA (blue bars) and 10 μM ABA (red bars; means \pm SEM, $n = 5$, with 7 seedlings/ n) normalized to the 0 μM ABA control conditions. G, Stomatal apertures 2 h after incubation in 0 μM ABA (blue bars) or 5 μM ABA (red bars; means \pm SEM, $n = 3$ with ≥ 12 stomata/ n) normalized to the 0 μM ABA control conditions. Statistical values for differences between Col-0 wild type and the *oip* mutant lines were calculated using a two-way ANOVA (P-values: *, < 0.05; **, < 0.01; ***, < 0.001).

A (OST1 and PP2A-subunit or ABI1 interactions)

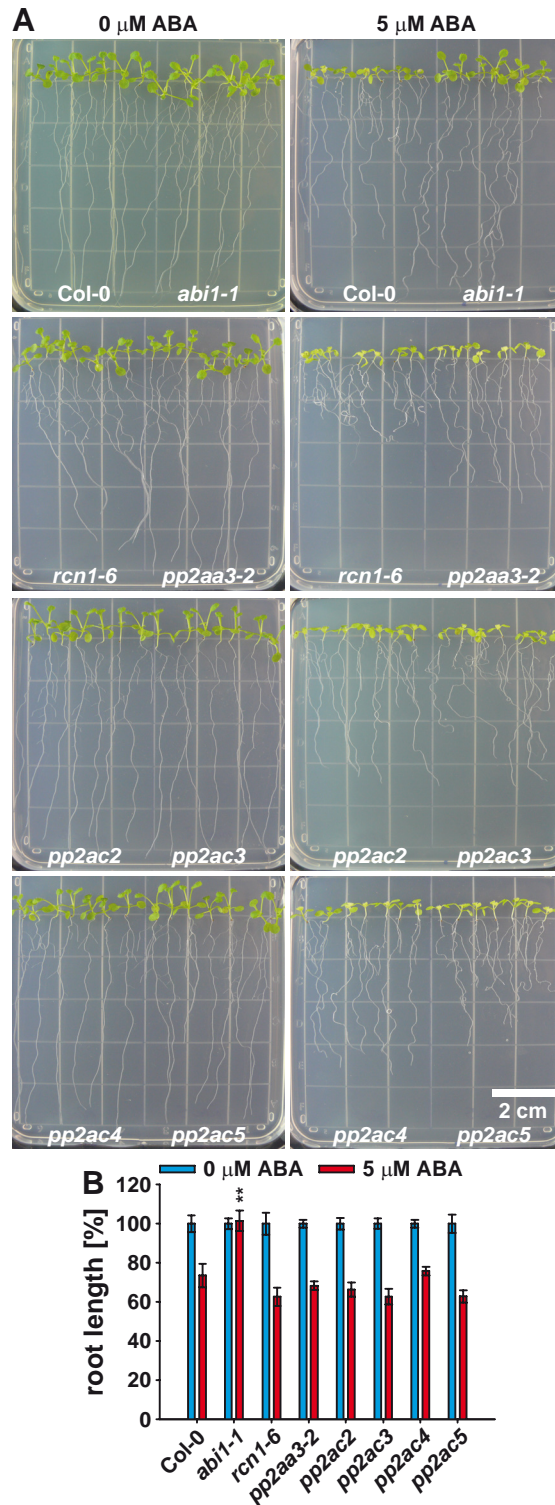


B (SnRK2 and RCN1 interactions)

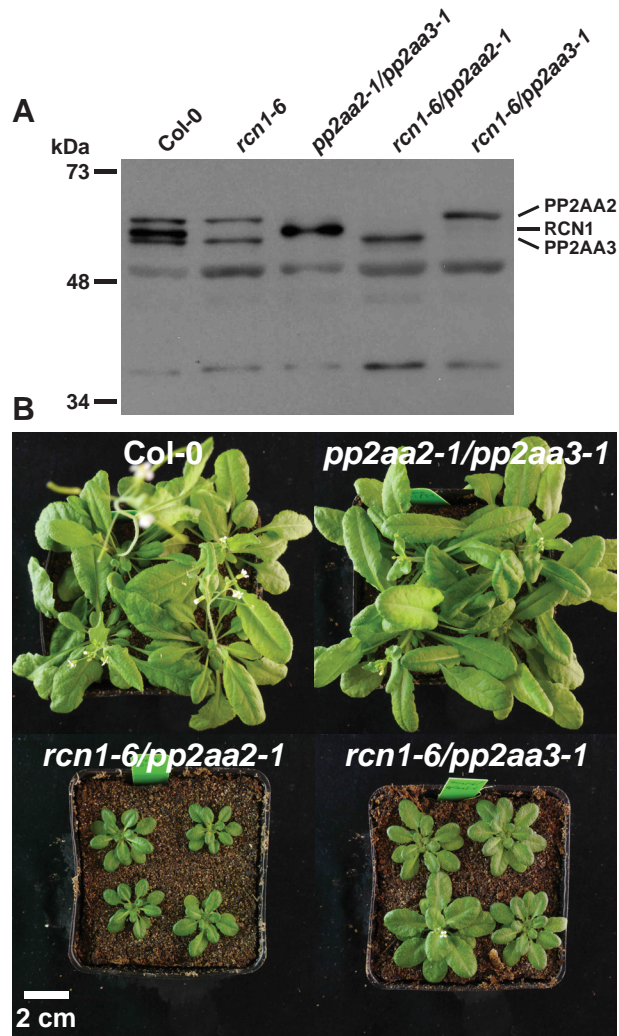
C (SnRK2 and PP2AB'beta)



Supplemental Figure S4. SnRK2-type protein kinases interact with PP2A-type protein phosphatase subunits in BiFC analyses. A and D, BiFC analyses of YN-OST1 with YC-PP2A-subunits and YC-ABI1 as control. B and E, BiFC analyses of YN-SnRK2s with YC-RCN1. C and F, BiFC analyses of YN-SnRK2s with YC-PP2AB'beta. A to C, High magnification 32-plane z-stack maximum projections with optimized brightness and contrast. Punctuate structures are indicated by an arrow. D to F, BiFC quantifications measured from entire low magnification images, which were acquired using identical settings for each experiment (means \pm SEM, n = 10 images). For better comparison of the emission signals the scale was adjusted in the inset of (D).

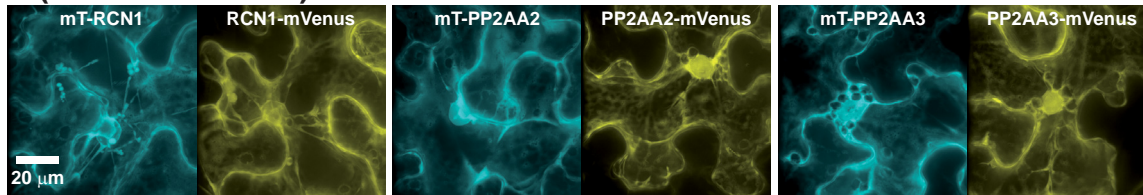


Supplemental Figure S5. ABA induces an enhanced root curling of *rcn1-6*. A, 4-day-old seedlings of Col-0, *abi1-1* in Col-0 background and *pp2a*-subunit single mutants were transferred to 0.5 MS agar plates supplemented with 0 μM ABA (left panel) or 5 μM ABA (right panel) and grown for additional 5 days. B, Root length of seedlings shown in (A) in the presence of 0 μM ABA (blue bars) and 5 μM ABA (red bars; means \pm SEM, $n = 4$ with 7 seedlings/ n) normalized to the 0 μM ABA control conditions. Statistical values for differences between Col-0 wild type and the investigated mutant lines were calculated using a two-way ANOVA (P-values: **, < 0.01).

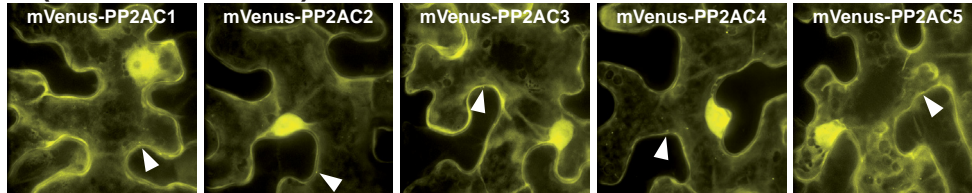


Supplemental Figure S6. Reduced expression of regulatory PP2AA-subunits affects plant growth. A, Immunoblot analyses of 6-day-old indicated lines probed with anti-RCN1 antiserum demonstrates the reduced expression of regulatory PP2AA-subunits in *pp2aa* single and double mutants. B, 39-day-old *rcn1-6/pp2aa2-1* and *rcn1-6/pp2aa3-1* plants exhibit a reduced growth when compared to Col-0 wild type and *pp2aa2-1/pp2aa3-1* plants.

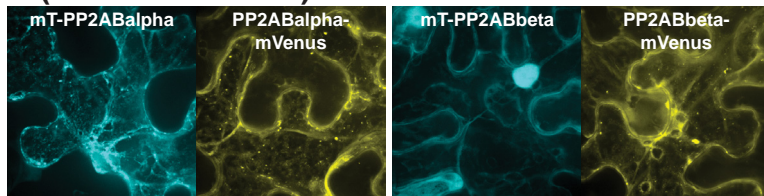
A (PP2AA-subunits)



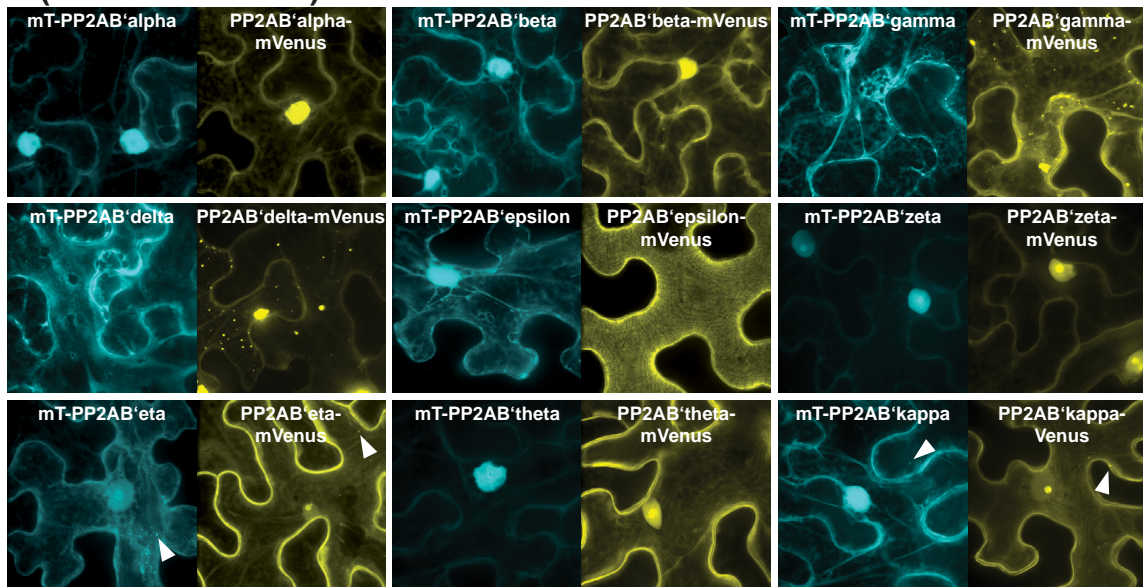
B (PP2AC-subunits)



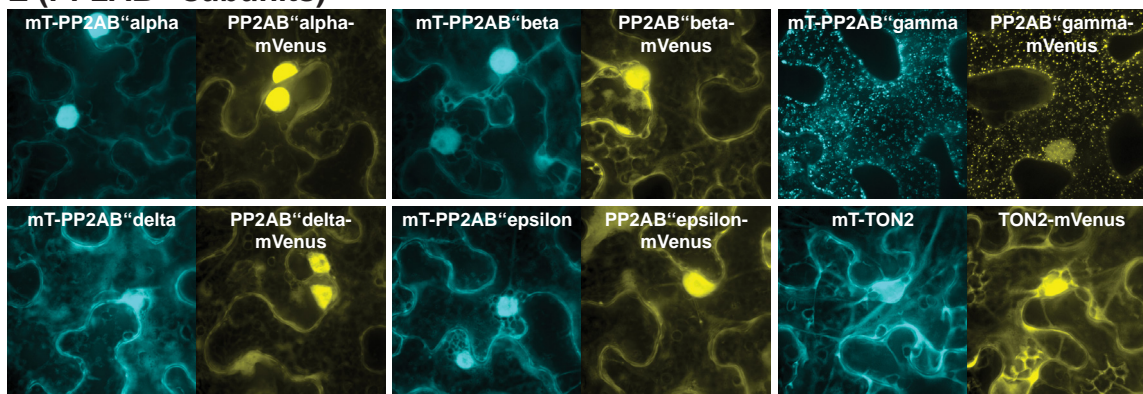
C (PP2AB-subunits)



D (PP2AB'-subunits)

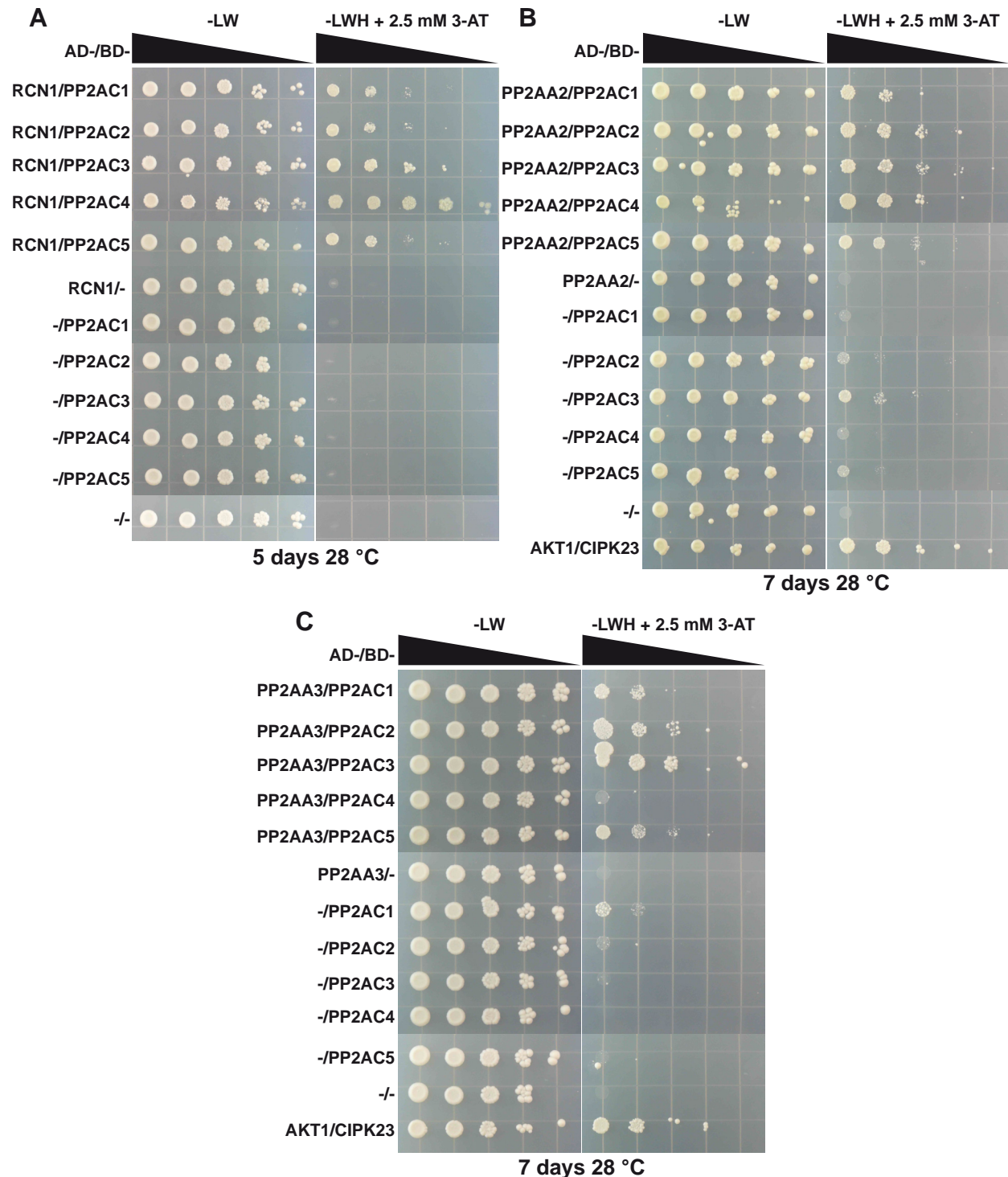


E (PP2AB''-subunits)



Supplemental Figure S7.

Subcellular localizations of PP2A-subunit fluorescent protein fusions. A to E, Maximum projections of 32-plane z-stacks of (m T) u r - quiose-PP2A-subunit (cyan), mVenus-PP2AC (yellow) and PP2A-subunit-mVenus fusion proteins (yellow). The fusion proteins analyzed are indicated. A, Regulatory PP2AA-subunits are localized in the cytoplasm and the nucleus. B, Catalytic PP2AC-subunits are localized in the cytoplasm, the nucleus and in punctuate structures (indicated by arrows). C, Regulatory PP2AB-subunits are localized in the cytoplasm, the nucleus and in punctuate structures. D, Regulatory PP2AB'-subunits are localized in the cytoplasm and the nucleus (B'alpha and B'beta), the cytoplasm and in punctuate structures (B'gamma and B'delta), the cytoplasm, nucleus and nucleolus (B'zeta) and the cytoplasm, nucleus, nucleolus, plasma membrane and punctuate structures (indicated by arrows; B'eta, B'theta, B'kappa). E, Regulatory PP2AB''-subunits are localized in the cytoplasm and the nucleus, except of B''gamma, which was observed in the nucleus and in punctuate structures.



Supplemental Figure S8. Regulatory PP2AA-subunits interact with catalytic PP2AC-subunits in yeast-two-hybrid analyses. A to C, Yeast-two-hybrid analyses of (A) RCN1 with PP2AC1-C5, (B) PP2AA2 with PP2AC1-C5 and (C) PP2AA3 with PP2AC1-C5. Indicated combinations of pGAD.GH-PP2AA-subunits and pGBT9.BS-PP2AC-subunits, empty plasmids and pGAD.GH-AKT1/pGBT9.BS-CIPK23 (Xu et al., 2006, positive control) were transformed into PJ69-4A. Decreasing 10-fold dilution series ($OD_{600\text{ nm}}$ of $10^0 - 10^{-4}$), indicated by the black arrows, were spotted onto -LW control media and onto -LWH + 2.5 mM 3-AT media to select for positive interactions and incubated for the indicated time period at 28 °C. Note that depending on the experiment, catalytic PP2AC-subunits exhibited a slight transactivation, as observed by a weak growth on selective media when yeast was transformed with empty pGAD.GH- and pGBT9.BS-PP2AC plasmids. However, in every case the selective growth of yeast transformed with pGAD.GH-PP2AA and pGBT9.BS-PP2AC plasmids was stronger than the respective transactivation controls.